J|A|C|S
ARTICLES
Published on Web 04/24/2004

Debundling and Dissolution of Single-Walled Carbon Nanotubes in Amide Solvents

C. A. Furtado,[||] U. J. Kim,[†] H. R. Gutierrez,[†] Ling Pan,[‡] E. C. Dickey,[§] and Peter C. Eklund*,[†,§]

Contribution from the Department of Physics, Materials Research Institute, and Department of Materials Science and Engineering, The Pennsylvania State University, University Park, Pennsylvania 16802, and Centro de Desenvolvimento da Tecnologia Nuclear − CDTN/CNEN, Belo Horizonte, MG, Brazil

Received November 13, 2003; E-mail: pce3@psu.edu

Abstract: Wet chemical methods involving ultrasound and amide solvents were used to purify and separate large bundles of single-walled carbon nanotubes (SWNTs) into individual nanotubes that could then be transported to silicon or mica substrates. The SWNTs studied were produced by the arc-discharge process. Dry oxidation was used in an initial step to remove amorphous carbon. Subsequently, two acid purification schemes were investigated (HCl- and HNO_3-reflux) to remove the metal growth catalyst (Ni−Y). Finally, ultrasonic dispersion of isolated tubes into either *N*,*N*-dimethylformamide (DMF) or *N*-methyl-2-pyrrolidone (NMP) was carried out. Raman scattering, atomic force microscopy (AFM), and electron microscopy were used to study the evolution of the products. Raman scattering was used to probe possible wall damage during the chemical processing. We found that both HCl and HNO_3 could be used to successfully remove the Ni−Y below ∼1 wt %. However, the HNO_3-reflux produced significant wall damage (that could be reversed by vacuum annealing at 1000 °C). In the dispersion step, both amide solvents (DMF and NMP) produced a high degree of isolated tubes in the final product, and no damage during this dispersion step was observed. HNO_3-refluxed tubes were found to disperse the best into the amide solvents, perhaps because of significant wall functionalization. AFM was used to study the filament diameter and length distributions in the final product, and interesting differences in these distributions were observed, depending on the chemical processing route.

Introduction

An effective chemical process to obtain clean, individual single-walled carbon nanotubes (SWNTs) in a stable solution is an important step needed for developing many large-scale applications for these molecular filaments, for example, as electrostatic shielding additives,[1] field emission flat panel displays,[2] radar paints,[3] conductive inks,[4] or in nanotube-polymer composites.[5] The strategies for the dissolution of SWNTs, or bundles of SWNTs, have involved either the supramolecular complexation of the tube walls with surfactants[6−8] or macromolecules,[9,10] or the functionalization of defect sites at the tube ends and side walls with amino groups and the subsequent conversion into derivatives, such as amides.[11,12] Finally, direct chemical functionalization of the side walls using addition reactions has been investigated.[13] Most of these moieties attached to the tube wall can be quite difficult to remove later and can also alter the SWNT physical and chemical properties. Furthermore, the chemical processing may damage the nanotube walls, that is, remove C-atoms from the graphene cylinder or

† Department of Physics, The Pennsylvania State University.
‡ Materials Research Institute, The Pennsylvania State University.
§ Department of Materials Science and Engineering, The Pennsylvania State University.
|| Centro de Desenvolvimento da Tecnologia Nuclear − CDTN/CNEN.

(1) Liu, C. Y.; Bard, A. J.; Wudl, F.; Weitz, I.; Heath, J. R. *Electrochem. Solid-State Lett.* **1999**, *2*, 577.
(2) (a) Rinzler, A. G.; Hafner, J. H.; Nikolaev, P.; Lou, L.; Kim, S. G.; Tomanek, D.; Colbert, D.; Smalley, R. E. *Science* **1995**, *269*, 1550. (b) Wang, Q. H.; Setlur, A. A.; Lauerhaas, J. M.; Dai, J. Y.; Seelig, E. W.; Chang, R. H. *Appl. Phys. Lett.* **1998**, *72*, 2912. (c) Choi, W. B.; Chung, D. S.; Kang, J. H.; Kim, H. Y.; Jin, Y. W.; Han, I. T.; Lee, Y. H.; Jung, J. E.; Lee, N. S.; Park, G. S.; Kim, J. M. *Appl. Phys. Lett.* **1999**, *75*, 20.
(3) Jensen, K. L. *Ultramicroscopy* **2003**, *95*, 29.
(4) Wei, C. Y.; Srivastava, D.; Cho, K. J. *Nano Lett.* **2002**, *2*, 647.
(5) (a) Treacy, M. M. J.; Ebbesen, T. W.; Gibson, J. M. *Nature* **1996**, *381*, 678. (b) Calvert, P. *Nature* **1999**, *399*, 210. (c) Ajayan, P. M.; Schadler, L. S.; Giannaris, C.; Rubio, A. *Adv. Mater.* **2000**, *12*, 750.
(6) Connell, M. J. O.; Bachilo, S. M.; Huffman, C. B.; Moore, V. C.; Strano, M. S.; Haroz, E. H.; Rialon, K. L.; Boul, P. J.; Noon, W. H.; Kittrell, C.; Ma, J.; Hauge, R. H.; Weisman, R. B.; Smalley, R. E. *Science* **2002**, *298*, 593.
(7) Vigolo, B.; Penicaud, A.; Coulon, C.; Sauder, C.; Pailler, R.; Journet, C.; Bernier, P.; Poulin, P. *Science* **2000**, *290*, 1331.
(8) Chen, R. J.; Zhang, Y.; Wang, D.; Dai, H. *J. Am. Chem. Soc.* **2001**, *123*, 3838.
(9) O'Connell, M. J.; Boul, P.; Ericson, L. M.; Huffman, C.; Wang, Y.; Haroz, E.; Kuper, C.; Tour, J.; Ausman, K. D.; Smalley, R. E. *Chem. Phys. Lett.* **2001**, *342*, 265.
(10) Star, A.; Stoddart, J. F.; Steuerman, D.; Diehl, M.; Boukai, A.; Wong, E. W.; Yang, X.; Chung, S.-W.; Choi, H.; Heath, J. R. *Angew. Chem., Int. Ed.* **2001**, *40*, 1721.
(11) Chen, J.; Hamon, M. A.; Hu, H.; Chen, Y.; Rao, A. M.; Eklund, P. C.; Haddon, R. C. *Science* **1998**, *282*, 95.
(12) Chen, J.; Rao, A. M.; Lyuksyutov, S.; Itkis, M. E.; Hamon, M. A.; Hu, H.; Chen, Y.; Cohn, R. W.; Eklund, P. C.; Colbert, D. T.; Smalley, R. E.; Haddon, R. C. *J. Phys. Chem. B* **2001**, *105*, 2525.
(13) Boul, P. J.; Liu, J.; Mickelson, E. T.; Huffman, C. B.; Ericson, L. M.; Chiang, I. W.; Smith, K. A.; Colbert, D. T.; Hauge, R. H.; Margrave, J. L.; Smalley, R. E. *Chem. Phys. Lett.* **1999**, *310*, 367.

functionalize the tube wall. Nanotube synthesis approaches that provide large quantities of unsupported, loose powders, or "soots" of SWNTs, such as the electric arc[14] or the HiPCO[15] process, also produce large bundles of SWNTs. Typically, each bundle might contain hundreds of nanotubes bound together by the weak van der Waals force. Unfortunately, the powders or soots from these procedures can (and usually do) contain significant quantities of metals (growth catalyst) as well as amorphous carbon; the amorphous carbon can also be present as a coating on the outside of the nanotube bundles. Information about the degradation of the structural order or chemical functionalization of the nanotubes can be extracted from Raman scattering spectra. Unfortunately, previous studies[16,17] to dissolve nanotubes in organic solvents, such as we investigate here, have not carried out spectroscopic investigation on their products, nor have they presented statistical information about the extent of the debundling, or the final length of the nanotubes. We were therefore motivated to initiate our own study to investigate these important issues.

In this paper, we present results from a systematic study on the effects of chemical processing of arc-derived bundles of carbon nanotubes to generate solutions containing individual SWNTs. The impact of our chemical and ultrasonic processing on the structural order of the nanotube has been studied by Raman scattering. We have considered several different process routes involving an initial dry oxidation step, a metal removal step in involving a reflux in HNO_3, HCl, or HCl/H_2SO_4, followed by a debundling/dispersion step in either *N*,*N*-dimethylformamide (DMF) or *N*-methyl-2-pyrrolidone (NMP), and then a final centrifugation step to separate the light and heavy fractures. Using atomic force microscopy (AFM), we have determined the distribution of the tubes/bundle and the average filament length for several process routes. Furthermore, we have examined whether chemically induced tube wall damage can be repaired by high-temperature heat treatment (HTT). The goal of our study was to obtain perfect dissolution of carbon nanotubes in an organic solvent, creating as little chemical damage to the nanotube wall as possible. Similar to the approach of Ruoff and co-workers,[16] we have used ultrasound to assist the debundling of the tubes and drive them into solution.

The polar, non-hydrogen-bonding Lewis bases, *N*,*N*-dimethylformamide (DMF) and *N*-methyl-2-pyrrolidone (NMP), have been investigated recently by Smalley and co-workers as solvents for breaking up bundles of SWNTs.[17] Based on AFM images in their report,[17] the suspension was found to contain some individual tubes and bundles of SWNTs. Statistical data on the length and diameter of the bundles or individual tubes were not provided.[17] In ref 17, a reflux in 2.6 M HNO_3 was used to remove metal and amorphous carbon from the nanotube soot before the dispersion into DMF. Monthioux et al.,[18] on the basis of transmission electron microscopy (TEM), reported that refluxing in 2.6 M HNO_3 damages the tube wall (presumably via the evolution of CO_2). Furthermore, they find that ultrasonic dispersion in DMF also seemed to increase the extent of the wall damage. These authors[18] also reported on the basis of TEM that structural defects resulting from the chemical processing can subsequently be removed by thermal annealing at high temperature.

Several procedures have been reported that address the purification of soots containing bundles of SWNTs.[19−21] To remove amorphous carbon, most of the procedures involve an initial oxidation step, that is, either via dry gaseous oxidation (in flowing dry air[22]) or by an oxidation in concentrated acids, for example, HNO_3,[19] or in hydrogen peroxide H_2O_2.[23] Typically, metals are subsequently removed by refluxing the oxidized soot either in HNO_3 or in HCl.[20] These processing steps can create wall defects, as suggested by Monthioux and collaborators,[18] and might also add oxygen-containing functional groups to the tube surface, for example, −COOH, −OH.[24] The presence of defects and surface functional groups on the bundle exterior can be useful, if their density and functionality can be controlled, as they provide surface sites for subsequent wall chemistry,[10,11] leading, for example, to better dispersion in solution. In previous studies on the purification of bundled SWNTs, we found using Raman scattering as a probe[20] that thermal oxidation in dry air, followed by HCl-based reflux to remove metals, is an effective, but "less aggressive", purification scheme, causing less wall damage than HNO_3 refluxing. Hence, in our efforts to produce isolated SWNTs in solution, we have explored two different acid treatments in the metal removal step (HNO_3 and HCl). In this work, we find that the extent of the damage and tube wall functionalization of isolated SWNTs in amide solvents depends mainly on the details of the acid purification step prior to the final "debundling" or "dispersion" step. We find no evidence that the ultrasonic dispersion step introduces additional wall defects or functionalization, as previously reported.[18]

Experimental Details

Arc-discharge soot (Carbolex, Inc.) produced using ∼4 atom % Ni−Y loaded carbon electrodes was studied here. The as-delivered material was found to contain bundles typically with ∼100s of SWNTs, ∼1−5 μm long, and with a mean nanotube diameter ∼1.4 nm, as determined by Raman-active radial breathing modes and HRTEM. Also present in the soot were ∼20−30 wt % amorphous carbon and ∼30 wt % of ∼20 nm diameter carbon-coated Ni−Y particles as determined by TGA in air. The carbon provides a rather robust chemical passivation coating over the metal impurity and prevents easy acid digestion of the Ni−Y in HCl.

Figure 1 shows a schematic diagram for our full purification and debundling process. The sample characterization performed after each step in the process is also indicated. First, we carried out a "dry" oxidation of the soot in air to "selectively" remove the amorphous

(14) (a) Ebessen, T. W.; Ajayan, P. M. *Nature* **1992**, *358*, 16. (b) Journet, C.; Maser, W. K.; Bernier, P.; Loiseau, A.; Chapelle, M. L. D. I.; Lefrant, S.; Deniard, P.; Lee, R.; Fisher, J. E. *Nature* **1997**, *388*, 756.
(15) Bronikowski, M. J.; Willis, P. A.; Colbert, D. T.; Smith, K. A.; Smalley, R. E. *J. Vac. Sci. Technol.* **2001**, *A19*, 1800.
(16) Ausman, K. D.; Piner, R.; Lourie, O.; Ruoff, R. S.; Korobov, M. *J. Phys. Chem. B* **2000**, *104*, 8911.
(17) Liu, J.; Casavant, M. J.; Cox, M.; Walters, D. A.; Boul, P.; Lu, W.; Rimberg, A. J.; Smith, K. A.; Colbert, D. T.; Smalley, R. E. *Chem. Phys. Lett.* **1999**, *303*, 125.
(18) Monthioux, M.; Smith, B. W.; Burteaux, B.; Claye, A.; Fisher, J. E.; Luzzi, D. E. *Carbon* **2001**, *39*, 1251.
(19) . (a) Rinzler, A. G.; Liu, J.; Dai, H.; Nikolaev, P.; Huffman, C. B.; Rodriguez-Macias, F. J.; Boul, P. J.; Lu, A. H.; Heymann, D.; Colbert, D. T.; Lee, R. S.; Fischer, J. E.; Rao, A. M.; Eklund, P. C.; Smalley, R. E. *Appl. Phys. A* **1998**, *67*, 29. (b) Hu, H.; Zhao, B.; Itkis, M. E.; Haddon, R. C. *J. Phys. Chem. B* **2003**, *107*, 13838.
(20) Harutyunyan, A. R.; Pradhan, B. K.; Chang, J. P.; Chen, G.; Eklund, P. C. *J. Phys. Chem. B* **2002**, *106*, 8671.
(21) Chiang, I. W.; Brinson, B. E.; Smalley, R. E.; Margrave, J. L.; Hauge, R. H. *J. Phys. Chem. B* **2001**, *105*, 1157.
(22) (a) Pradhan, B. K.; Harutyunyan, A. R.; Eklund, P. C. PSU Invention Disclosure, 2001; No. 2001−2445. (b) Sen, R.; Rickard, S. M.; Itkis, M. E.; Haddon, R. C. *Chem. Mater.* **2003**, *15*, 4273.
(23) Zhou, O.; Shimoda, H.; Gao, B.; Oh, S.; Fleming, L.; Yue, G. *Acc. Chem. Res.* **2002**, *35*, 1045.
(24) Zhang, J.; Zou, H.; Qing, Q.; Yang, Y.; Li, Q.; Liu, Z. *J. Phys. Chem. B* **2003**, *107*, 3712.

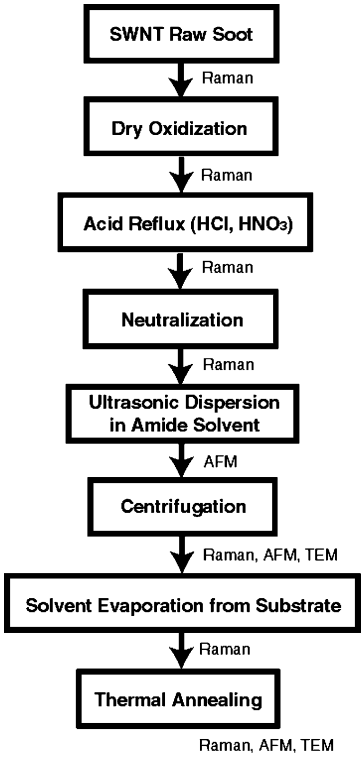

Figure 1. Schematic diagram for the carbon nanotube debundling and dissolution process. The sample characterization performed after each step in the process is indicated.

carbon. In reality, we strive to create conditions that promote a significantly more rapid oxidation of amorphous carbon relative to that of SWNTs. Conditions (temperature/time) for this process were found by thermogravimetric analysis (TGA; TA Instruments, model SDT 2960). The time and temperature in the thermal oxidation process are somewhat different for each sample batch. It was determined that a thermal soak of the CarboLex soot at 365 °C for 90 min in a flow of dry air (100 sccm) was required to achieve selective oxidation of the amorphous carbon, minimizing nanotube mass loss. If dry oxidation is done carefully, only ~10% of the SWNTs are lost during this step. Importantly, the carbon coating on the metal particles is also weakened during this step.[20] Using the optical density (OD) obtained from NearIR−vis−UV spectroscopy, Haddon's group evaluated the purity of their chemically processed SWNT soot (bundled SWNTs + amorphous carbon + catalyst). Their figure of merit was essentially the ratio of the integrated intensity of the interband peak associated with the SWNT E_{22}'s to that of the linear background identified with an amorphous carbon component. What they observed was a significant reduction in the linear background contribution processing in either dry oxidation (~400 °C)[19b] or HNO_3-reflux,[22b] indicating a reduction in the amorphous carbon in the sample. It is not clear to us that the SWNTs themselves will not also provide a linear background due to high energy $\pi-\pi^*$ transitions away from the van Hove singularities. We also investigated the effect of oxidation and acid reflux on the NearIR−vis−UV OD and found a reduction in the linear background term upon chemical processing (cf., Supporting Information S1). However, our reduction in background was not as significant as they reported.

Next, we removed the metal (Ni−Y) by a reflux in acid solution, using either a strongly oxidizing 3 N HNO_3 solution for 16 h or a weakly oxidizing 6 N HCl solution for 24 h. The solid residues, including the SWNT bundles, were then trapped by vacuum filtration on a 5 μm pore size polycarbonate membrane filter (Whatman, Inc.). With the filter still in place, the filtrate was washed with about 2 L of hot deionized water. The solution in the bottom container of the vacuum filtration apparatus was observed to be light in color. Next, ~3 mL of pH 10 NaOH solution was poured over the filtrate to reduce its acidity. After NaOH passed through the filter, ~50 mL of hot deionized water was then poured over the filtrate in the funnel, and litmus paper was used to check the pH in the funnel. The NaOH wash and pH check were repeated until the pH was ~7. For HCl-treated samples, the neutral solution above the filtrate was observed to be light gray, but for HNO_3-treated samples, this solution was black. The black coloration has been attributed[19] to the solubilization of small polycyclic aromatic sheets and occurs in neutral and moderately basic aqueous solutions after their functionalization with carboxyl groups by nitric acid oxidation. The larger (presumably), carboxylic-functionalized nanotube bundles are contained in the filtrate. The light gray color for the solution derived from HCl-treated samples is identified with the solubilization of small amounts of the carbonaceous materials oxidized and functionalized during our dry gaseous oxidation step. After removal of most of the small nanoparticulate impurities by the NaOH wash, we find that the filtrate contained a significantly lower total mass yield after HNO_3-refluxing than after HCl-refluxing.

Ultrasound was then used to disperse and debundle the purified SWNT bundles in amide solvents. Careful comparison of the benefits of two amide solvents mentioned in the literature as useful in dispersing SWNTs was investigated, that is, DMF and NMP (Aldrich, Inc., Spectral Grade). A mass of 0.02 mg of SWNT was added per milliliter of solvent. Typically, ultrasonic dispersion was carried out for 4 h in a low power bath (Aquasonic, Inc., model P250HT). The solutions were then immediately centrifuged (Eppendorf, Inc., model 5417C) at 14 000 rpm (20 800*g*) for 90 min, and the supernatant liquid containing the debundled SWNTs was withdrawn for study. The centrifugation step was found important for removing large particles (amorphous carbon, multishell carbon, etc.) and the few large (>5 nm) bundles that may remain. The quality of the dispersion of isolated tubes in DMF or NMP was examined by both atomic force microscopy (AFM) using a Digital Instruments Nanoscope (model IIIA) and also via transmission electron microscopy (TEM; JEOL 2010F; 100 kV). Samples for AFM were prepared by depositing a drop of solution between two freshly cleaved mica substrates that were then allowed to dry in contact in air for 12 h. The substrates were then separated for AFM studies. Using this preparation, we found that a uniform submonolayer distribution of SWNTs is distributed across the face of both mica substrates. The measured standard deviation in the height of a single filament on the mica was determined to be $\sim \pm 0.1$ nm, as determined by measuring the height at several points along the same filament. Several images taken from different regions of the mica were evaluated to obtain a statistically reliable estimate for the fraction of filaments identifiable as individual tubes or containing 2, 3, or >3 tubes per bundle. TEM grids were prepared by placing a drop of the amide/SWNT solution on a "lacey carbon" grid.

Samples for Raman scattering studies were prepared by placing a few drops of amide/SWNT solution on a warm ~60 °C silicon substrate. The possible benefits of a high-temperature annealing (1100 °C in a vacuum) to restore structural order in the debundled and dispersed SWNTs was also studied by simply heating several of the Si substrates in flowing argon gas or high vacuum. Micro-Raman spectra were collected using a triple-grating Micro-Raman spectrometer (JY Horiba, model T64000) equipped with a confocal microscope (Olympus BH-2) and a CCD detector. The scattering was excited using an argon ion laser (488 nm), and the power measured at the sample was 1 mW inside a ~1 μm laser spot size. This particular excitation wavelength primarily couples to the semiconducting tubes in the sample.[25,26]

(25) Dresselhaus, M. S.; Dresselhaus, G.; Pimenta, M. A.; Eklund, P. C. In *Analytical Applications of Raman Spectroscopy*; Pelletier, M. J., Ed.; Blackwell Science: Cambridge, MA, 1999; Chapter 9.
(26) Saito, R.; Kataura, H. In *Carbon Nanotubes: Synthesis, Structure, Properties and Application*; Dresselhaus, M. S., Dresselhaus, G., Avouris, Ph., Eds.; Springer-Verlag: Berlin, 2001.

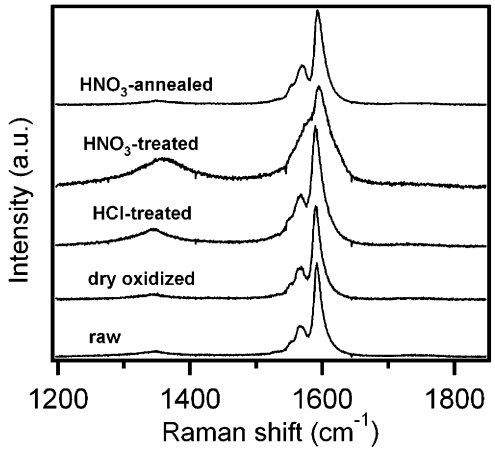

Figure 2. Raman spectra showing D-band (~1350 cm^{-1}) and the G-band features (~1590 cm^{-1}) of (a) arc-discharge raw soot, (b) dry-oxidized SWNTs, (c) HCl-purified SWNTs, (d) HNO_3-purified SWNTs, and (e) HNO_3-purified SWNTs after annealing at 1100 °C under vacuum (10^{-6} Torr). E_{laser} = 2.41 eV (488 nm). There is an arbitrary vertical scale for each spectrum.

Results and Discussion

Purification. Using TGA in flowing dry air (100 sccm, 5 °C/min heating to 800 °C), the raw CarboLex arc-discharge SWNT soot was found to contain ~20−30 wt % SWNT and ~30−40 wt % Ni−Y. This conclusion was reached by both observing the oxidative mass loss of amorphous carbon at low *T* (350−375 °C) and attributing the final sample mass at 800 °C in air to metal oxides. After a two-step purification process (dry oxidation followed by acid reflux), the wt % of nanotubes in the sample increased to approximately 90% (HNO_3) and 85% (HCl); the remainder of the solids at this stage of purification was typically ~8−12 wt % amorphous carbon, and ~1−2 wt % metal.[27]

Room-temperature Raman spectra (488 nm excitation) of SWNT material at various stages of the chemical processing are shown in Figure 2. From bottom to top in the figure are the high-frequency spectra for the following: as-prepared or raw arc soot (a), dry-oxidized soot (b), dry-oxidized soot + HCl-reflux (c), dry-oxidized soot + HNO_3-reflux (d), and dry-oxidized soot + HNO_3-reflux + high *T* annealing (e) (annealed for 1 h under vacuum (10^{-6} Torr) at 1100 °C).

Two Raman bands are typically observed for sp^2 carbon material in the 1200−1850 cm^{-1} range;[25,26,28,29] that is, a relatively broad, disorder-induced band (or "D-band") appears in the region 1300−1370 cm^{-1}, and a first-order-allowed band with substructure appears in the region ~1580−1600 cm^{-1}. In graphite, a single high-frequency band (or "G-band") appears in the Raman spectrum at 1582 cm^{-1} and is associated with the E_{2g} symmetry long wavelength optical phonon ($q = 0$).[25] The line shape of the G-band in highly crystalline graphite is Lorentzian (full width at half-maximum (fwhm) ≈ 6 cm^{-1}). For small diameter carbon nanotubes ($d < 2$ nm), the cylindrical and chiral (*n*,*m*) symmetry produces Raman activity in related vibrations with frequencies in the range 1450−1620 cm^{-1}. Several of these modes are observed as unresolved sidebands to the main peak at 1591 cm^{-1}.[25,28] In the bottom three spectra of Figure 2, for example, one can easily observe one main peak (1591 cm^{-1}) and two unresolved bands on the low-frequency side of the main peak. Actually, to fit the complex band shape of the nanotube G-band, a fourth high-frequency, unresolved Lorentzian peak at ~1610 cm^{-1} is also required. The effects on the high-frequency Raman spectrum of carbon nanotubes due to wall disorder and chemical functionalization can be anticipated. These chemical changes are expected to broaden the structure in the G-band and to increase the integrated intensity and width of the D-band.[25,26,29]

Carbon nanotubes also exhibit a unique, low-frequency, first-order Raman scattering feature identified with the radial breathing mode of the tube wall. The frequency of this mode is inversely related to the nanotube diameter *d*. An approximate expression based on several experiments and theory is given by $\omega = 234\ cm^{-1}\cdot nm/d$.[30] In a real sample consisting of tubes with many chiralities (*n*,*m*), a particular excitation wavelength will resonate with a subset of the tubes, and radial modes associated with these tubes will form an R-band. Structure within this band can be identified with individual tubes whose diameter *d* is related to a mode frequency via the empirical relationship mentioned above. In the raw CarboLex arc material, the main peak in the R-band is located at ~161 cm^{-1}. This corresponds to a tube diameter of 1.4 nm.

The D-band is a special mode; it is called a "dispersive" band. This terminology means that the position of the Raman band depends on the excitation frequency.[31,32] The movement of the D-band position with excitation frequency depends on the details of the excitation and the wave vector of the phonon mode being excited. The D-band is present in all known forms of disordered sp^2 carbons and has been identified with C-atom vacancies, substitutional impurities (boron), finite grain or particle effects, or any other symmetry-breaking phenomena.[25,31] We therefore need to be extremely careful using the D-band to assess damage to the SWNTs caused by the purification process.[25] For example, a contribution to the D-band spectrum can come from minority phases of disordered sp^2 carbon in the sample (Figure 2a). After dry oxidation of the sample to remove the amorphous carbon (Figure 2b), the relative intensity of the D-band is observed to decrease very slightly. However, after the acid treatment (second step of the purification process), the relative integrated intensity of the D-band intensity increases, and the D-band broadens (Figure 2c and d). This is particularly evident for the HNO_3-refluxed material. Because the TGA data suggest that most of the amorphous carbon has been removed from the sample in the dry oxidation step[33] and the NaOH wash removes oxidized carbonaceous materials derived from dry or acid oxidation, we interpret the increase of the D-band intensity and width after acid treatment as evidence for a decrease in structural order in the SWNT bundles as a result of the refluxing. After acid treatment, the intensity of the D-band relative to the G-band

(27) Increasing the dry oxidation time and the reflux time can reduce the wt % metals to ≪1 wt %. Also, selective microwave heating followed by 6 h refluxing in 4 N HCl was found previously to reduce the metal content to a few tenths of a wt % (see ref 20).

(28) Rao, A. M.; Richter, E.; Bandow, S.; Chase, B.; Eklund, P. C.; Williams, K. A.; Fang, S.; Subbaswamy, K. R.; Menon, M.; Thess, A.; Smalley, R. E.; Dresselhaus, G.; Dresselhaus, M. S. *Science* **1997**, *275*, 187.
(29) Dresselhaus, M. S.; Dresselhaus, G.; Jorio, A.; Souza Filho, A. G.; Saito, R. *Carbon* **2002**, *40*, 2043.
(30) Chen, G.; Bandow, S.; Margine, E. R.; Nisoli, C.; Kolmogorov, A. N.; Crespi, V. H.; Gupta, R.; Sumanasekera, G. U.; Iijima, S.; Eklund, P. C. *Phys. Rev. Lett.* **2003**, *90*, 257403.
(31) Pimenta, M. A.; Jorio, A.; Brown, S. D. M.; Filho, A. G. S.; Dresselhaus, G.; Hafner, J. H.; Lieber, C. M.; Saito, R.; Dresselhaus, M. S.; Endo, M. *Phys. Rev. B* **1999**, *59*, R6585.
(32) Mattheus, M. J.; Pimenta, M. A.; Dresselhaus, G.; Dresselhaus, M. S.; Endo, M. *Phys. Rev. B* **2000**, *64*, R041401.

was always found to be higher for the HNO_3-treated samples than for the HCl-treated samples. Using the D-band as a probe, it is clear from comparing the spectra in Figure 2c (HCl-reflux) and Figure 2d (HNO_3-reflux) that HNO_3 induces significantly more chemical change to the dry-oxidized nanotubes. In addition to the difference in the D-band intensity, we can also see in Figure 2c,d that the features in the G-band are also broadened as a result of refluxing. For the case of HCl-reflux, the effect is somewhat subtle, yet it can be observed with careful curve fitting. In the case of HNO_3-reflux, however, the broadening is obviously quite strong, and the substructure within the G-band almost disappears. We believe that it is very significant that in the case of HCl-reflux, no significant change in the fwhm for the G-band was observed. For the HNO_3-treated sample, a fit to the experimental G-band shows the presence of a new Raman peak near ~1620 cm^{-1}. The unresolved shoulder near ~1620 cm^{-1} has a counterpart in disordered sp^2 carbons and is referred to in the literature as the G*-band.[25,26] The frequency of the G*-band in graphite corresponds to the mid-zone maximum in the phonon density of states in the optical branch.[25] As structural disorder tends to introduce structure in the Raman spectrum near positions of maxima in the one-phonon density of states of the ordered (parent) material, the G*-band is therefore another anticipated signature of wall disorder, or functionalization or wall defects after processing.

There have been several reports that chemical oxidation and processing leads to the formation of oxygen-containing functional groups on the tube walls, such as carboxylate, hydroxyl, ether, and quinone groups, etc.[24,34−36] The fractional abundance of each of these functional groups is variable and should depend on the details of the particular chemical process. For the HNO_3-based treatment, carboxylic groups have been reported as the most abundant functional group on the carbon nanotube surface.[24,35] The details of the mechanisms behind the chemical disruption of the π-bonding in graphene or SWNT are still under study. Using infrared spectroscopy, Zhang et al.[24] have proposed that the oxidation process begins with the oxidation of initial wall defects (step 1) (e.g., at $-CH_2$ and $-CH$ groups, or pentagon−heptagon pair defects). These defects might be present, to some extent, after growth, that is, before chemical processing or produced by processing. After these defects are oxidized, they have suggested two more successive steps in the evolution of the defect structure: the defect-generating step (step 2) and the defect-consuming step (step 3). In step 2, an electrophilic addition to the wall begins at the bond defined by

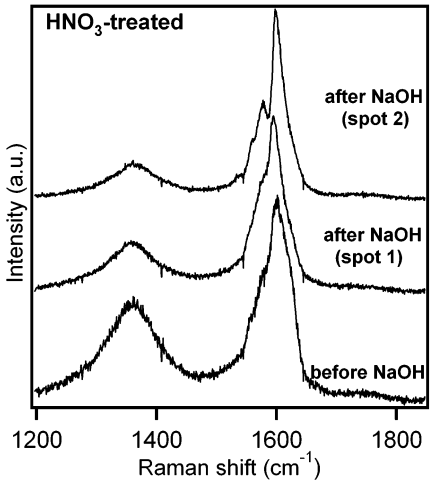

Figure 3. Raman spectra for HNO_3-purified SWNT sample before (a) and after (b,c) neutralization with pH 10 NaOH solution. The sample heterogeneity after removing bulk impurities is characterized by significant spot-to-spot variation in the G-band features as noted in the different spectra (b) and (c).

the fusion of adjacent six-membered rings in the wall, generating more active sites, such as −OH and −C═O. The third, or final step, is the defect-consuming step (step 3), whereby the graphene structure of the wall is locally destroyed by the oxidation of the generated active sites in steps 1 and 2. According to Zhang et al.,[24] steps 2 and 3 compete and cooperate with each other; they require special, strong oxidation conditions. According to these authors, refluxing in dilute (2.6 M) nitric acid under conditions (3 M) similar to those used here should be considered a mild oxidation for SWNT, introducing carboxylic groups only at defects that existed prior to chemical processing. Also, according to their work,[24] extended refluxing in dilute (2.6 M) HNO_3 for >96 h appears to have no impact on the generation of new defect sites on the tube wall, and they propose that this extended HNO_3 digestion advances the system only as far as step 1 (above); the oxidation does not proceed to steps 2 and 3. However, in this work, our Raman scattering spectra show that dilute (3 N) HNO_3-reflux for ~16 h has a significant impact on the tube wall structure. We therefore suggest that even mild HNO_3 treatments can create defect sites on the wall.

Our Raman microprobe has a spatial resolution of 1 μm, and using this resolution we can observe a highly heterogeneous character for the HNO_3-refluxed sample. The HCl-refluxed material is, by comparison, very homogeneous. In Figure 3, we show the Raman spectra for the HNO_3-treated sample before neutralization (washing) with NaOH, and also the Raman spectrum from two nearby spots of the sample after neutralization with NaOH. As discussed in the previous section, the neutralization with NaOH removes nanoparticulate impurities by solubilizing the carboxylic acid-functionalized carbonaceous materials.

As a consequence of their removal from the sample, one would expect the contributions of disordered nanoparticulate carbons and small polycyclic sheets to the D- and G*-band to be decreased. The anticipated outcome of their removal is seen in the Raman spectrum of spot 2 in Figure 3, but not for spot 1 on the same sample. This sample heterogeneity was also observed in TEM images, as discussed by other authors.[18]

It is interesting to observe that chemical changes and structural damage induced by HNO_3-reflux is largely reversible at

(33) The initial (raw material) and residual (after purification) amount of amorphous carbon and catalyst in the Crabolex samples were determined by temperature-programmed oxidation (TPO) using a TA Instruments SDT 2960 thermogravimetric analyser. The Carbolex sample was maintained in a flow of dry air at 100 sccm, while the temperature was ramped linearly in time (5 °C/min) from room temperature to 800 °C. The temperature (T) [or time (t)] dependence of the evolution of the sample mass m is measured. With increasing T, carbon is converted to CO/CO_2, metal is converted to an oxide, and $m(T)$ decreases. Characteristic combustion temperatures of the various carbon phases in the soot, for example, amorphous carbon, SWNT, multishell carbon, can be identified by the peak positions in the derivative data (DTPO), that is, dm/dT versus T data. The area sob each peak in the DTPO curve can be used as an estimate of the relative amount of the various carbon phases. As an example of this procedure, see ref 20.

(34) Niyogi, S.; Hamon, M. A.; Hu, H.; Zhao, B.; Bhowmik, P.; Sen, R.; Itkis, M. E.; Haddon, R. C. *Acc. Chem. Res.* **2002**, *35*, 1105.

(35) Kuznetsova, A.; Popoya, I.; Yates, J. T.; Bronikowski, M. J.; Huffman, C. B.; Liu, J.; Smalley, R. E.; Hwu, H.; Chen, J. G. *J. Am. Chem. Soc.* **2001**, *123*, 10699.

(36) Liu, J.; Rinzler, A. G.; Dai, H. J.; Hafner, J. H.; Bradley, R. K.; Boul, P. J.; Lu, A.; Iverson, T.; Shelimov, K.; Huffman, C. B.; Rodriguez-Macias, F.; Shon, Y. S.; Lee, T. R.; Colbert, D. T.; Smalley, R. E. *Science* **1998**, *280*, 1253.

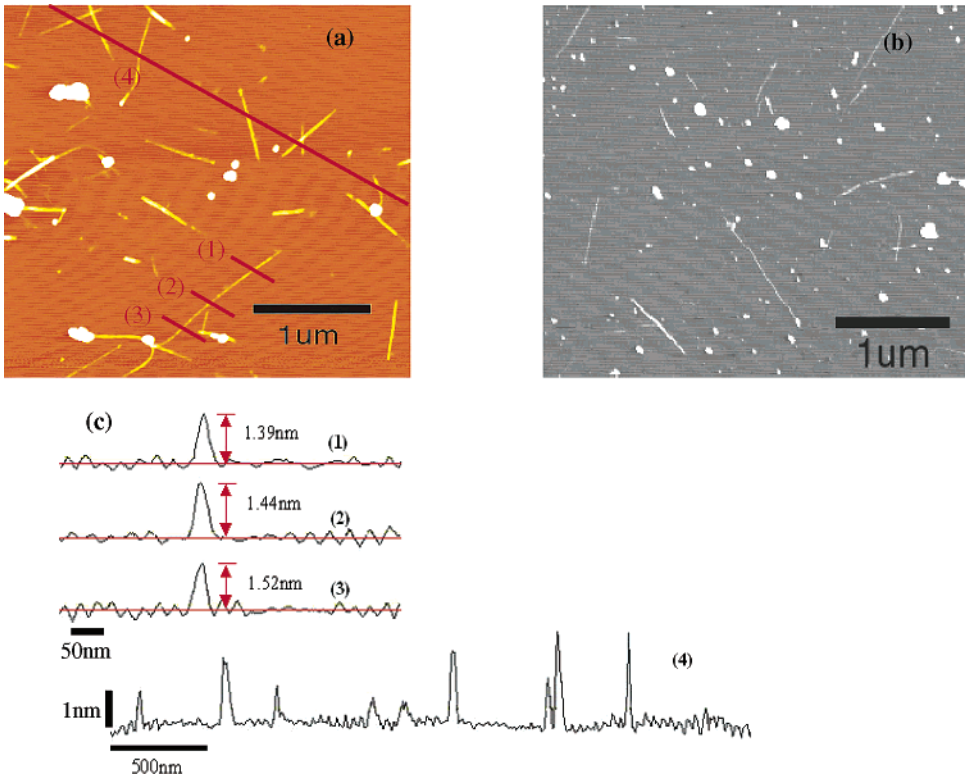

Figure 4. Typical AFM images showing the dispersion of SWNTs in DMF for (a) HCl-treated and (b) HNO_3-treated SWNT material. (c) Shows z-scan analysis of the lines labeled (1), (2), (3), and (4) in (a).

moderate temperatures. By annealing the refluxed material at ~1100 °C under vacuum, or in argon, the tube wall disorder is largely repaired. We present that chemical functional groups associated with wall defects are also removed. This can be seen by comparing the Raman spectrum in Figure 2e (annealed) to that after refluxing (Figure 2d). For example, after annealing, we find that the G*-peak at 1620 cm^{-1} disappears and that the D- and G-band's positions, widths, and relative intensities return to those observed for the SWNTs in raw soot (Figure 2a).

Debundling and Dispersion into Organic Solvents. The final step of the chemical processing to produce individual (debundled) SWNTs involves the dissolution of the nanotube bundles into individual tubes in an organic solvent. Previous authors have found that this debundling or "dispersion" requires ultrasonic assistance.[16,17,36] Furthermore, it has been reported that ultrasonic dispersion in DMF introduces further damage to the tube walls.[18] We have investigated this contention using Raman scattering and have tried to correlate any ultrasonic-related wall damage with the purification protocol prior to the debundling and dissolution step. To examine these phenomena, samples of purified bundled tubes were ultrasonically agitated in DMF or NMP for 4 h. Longer sonication times were found to have no additional benefit on the dispersion. Afterward, centrifugation was performed at 14 000 rpm (20 800*g*) for 90 min and resulted in transparent, light-gray suspensions; most large particles and any remaining larger bundles were driven out of solution. The centrifugation step was used to remove large particles (i.e., 20 nm diameter particles) and large diameter bundles from solution (i.e., $d \geq 5$ nm). We estimate that ~15% of the SWNTs are removed as small bundles by centrifugation. The suspensions were observed to be stable; no evidence for agglomeration was observed over periods of weeks. Interestingly, if the SWNT soot was subjected only to dry oxidation (no acid reflux), we found that the amide solvent with sonication produced no measurable dispersion; no isolated tubes could be found in solution. This observation may suggest that the catalyst particles serve as an important anchor at one end of the bundle, encouraging rebundling in the absence of ultrasonic agitation. The reason that both dry oxidation and acid reflux (either HCl or HNO_3) are a required first step prior to ultrasonic debundling in the amides remains (for us) an interesting point that we cannot yet fully explain. On the basis of intercalation studies in graphite, one would not expect HCl to intercalate into the SWNT bundle (i.e., HNO_3 forms a graphite intercalation compound, and HCl does not). Nevertheless, both the HCl- and the HNO_3-treated SWNT bundles can be efficiently debundled in amide solvents. This suggests (to us) that HCl can also penetrate the SWNT bundles and the result of this penetration is to reduce the van der Waals interaction between tubes in a bundle, allowing the amides to penetrate the bundle via a displacement reaction. We suggest that ultrasound and weak charge transfer between the amide and the SWNT, and a reduced van der Waals interaction (perhaps) driven by acid penetration into the bundle, may all be required to drive an efficient debundling process. Figure 4a,b shows topographic AFM images of carbon nanotubes deposited from DMF solution onto cleaved mica substrates. The same AFM tip was used to acquire both parts a and b. As the tip scans over a nanotube filament, we can estimate the filament diameter via the change in the height of the tip. The diameter of all filaments for the histogram was checked at the different positions along the filaments at least three times. We will show histograms of filament diameter and length below. The apparent width of the filaments in the figure is not significant; changes in the width at the real scale of the nanotube diameter are not resolvable with these AFM tips. In Figure 4a and b, we show, respectively, the images for dry oxidized nanotube bundles

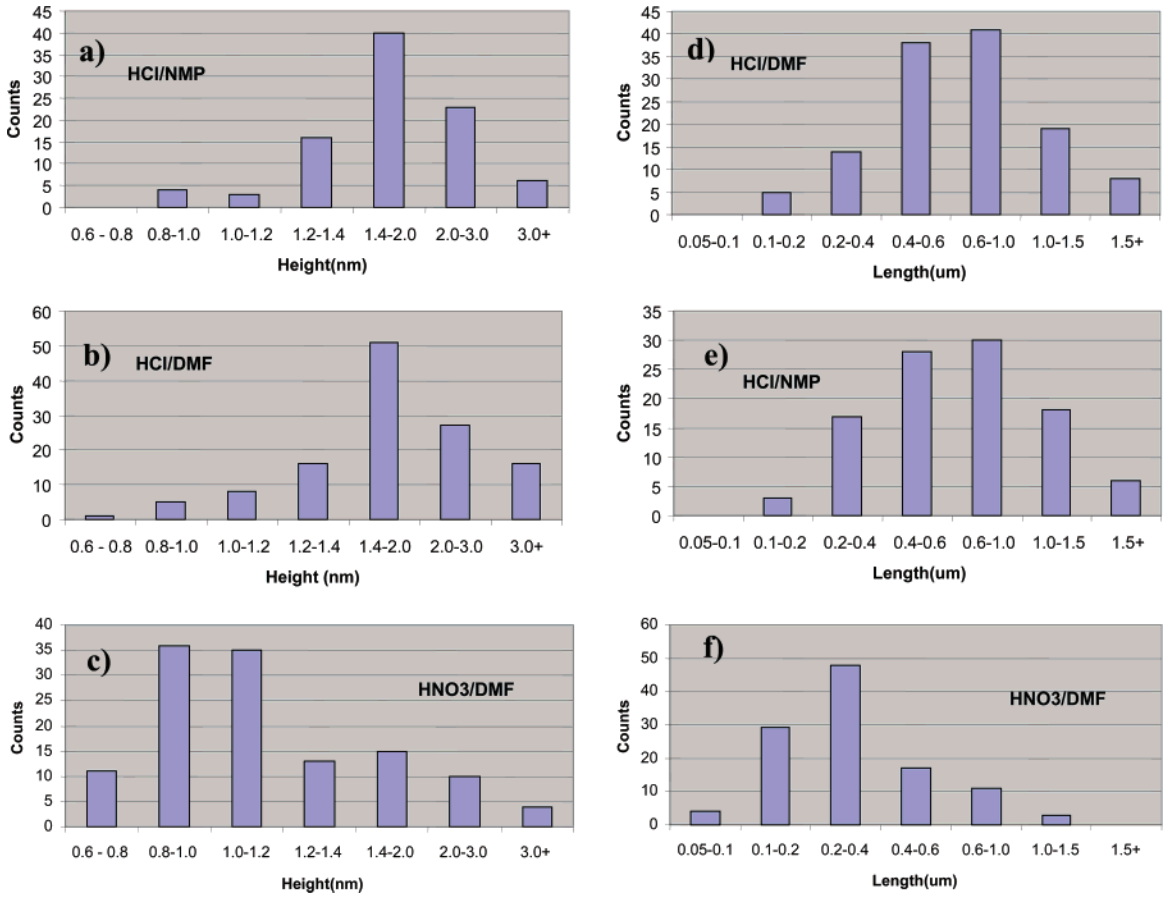

Figure 5. AFM diameter and length distributions for arc-derived SWNTs after various purification and debundling processes.

refluxed in HCl (a) and HNO_3 (b). Figure 4c shows z-scan analysis of the lines labeled as (1), (2), (3), and (4) in Figure 4a. In Figure 4c, the data for lines (1), (2), and (3) all refer to the same tube. The actual filament diameter measured in three locations is shown. The average filament diameter in this case is $\bar{d} = 1.45 \pm 0.07$ nm. The line labeled as (4) in Figure 4a cuts across 7 tubes and 2 small particles, and the z-scan is also shown in Figure 4c; examples of isolated tubes and very small bundles (2−3 tubes/one bundle) can be seen. By comparing the topographic results in Figure 4a and b, several results can be seen immediately: (1) HNO_3-reflux (Figure 4b) has produced a better dispersion; that is, more of the filaments are actually individual SWNT; and (2) the average length of the filaments is slightly shorter when processed with HNO_3 than with HCl. A closer inspection of many of the filament's topology (via z-scan) showed the following. For the HCl-refluxed sample in DMF, we observed that the apparent thickness of some of the isolated tubes was not uniform along the tube length, suggesting a coating had formed; this coating was definitely less than one-half a tube diameter in thickness.

Also, on occasion, small bundles of 3−6 tubes processed with HCl/DMF were observed that exhibited a tapering along their length. We suppose that this might be caused by the fact that not all tubes in these small bundles were cut at the same position.

To see the real effects of various chemical process schemes on the nanotube dispersion, we have made a detailed AFM study of various topographic images such as those shown in Figure 4a,b to obtain the distribution of filament height (diameter) and filament length for several purification/debundling processes. All of the samples stemmed from the same batch of CarboLex nanotube soot. The results are shown in Figure 5 for the processing indicated; the three left-hand panels (Figure 5a−c) and the three right-hand panels (Figure 5d−f) refer, respectively, to the filament diameter and length distributions. As can be seen, the filament diameter distributions produced via HCl/DMF and HCl/NMP are remarkably similar; both exhibit a peak in the bin (1.4−2.0 nm), consistent with the average diameter (∼1.4 nm) reported for CarboLex tubes. Interestingly, the AFM data in Figure 5c indicate that small diameter tubes are more commonly found after the HNO_3/DMF process than after the HCl/DMF or HCl/NMP processes. The reason for this is not clear, but we speculate it may have something to do with the higher reactivity of smaller diameter nanotubes in HNO_3.[34] It may be that HNO_3 refluxing preferentially functionalizes smaller diameter SWNTs, causing bundles containing them to be preferentially exfoliated. From Figure 5a−c, we can see that both HCl- and HNO_3-refluxed material can be dispersed successfully in DMF or NMP, as bundles containing more than 3 tubes per bundle were rarely detected, but the HNO_3/DMF process is the most successful at generating individual tubes in solution. This better dispersion does come at a price, as Raman scattering indicates that the HNO_3-reflux produces considerably more wall damage (Figure 2d).

We can define a quantitative measure of the success in debundling or dispersion by a "dispersion yield" (Y_D), defined as the fraction of the nanotubes found in the final solution as individual nanotubes. From data in Figure 5a−c, we find $Y_D \approx$ 50% for HCl/(DMF or NMP) and $Y_D \approx 90\%$ for HNO_3/DMF. Also, we should add that comparing AFM z-scan data for sonicated solutions with and without the added centrifugation

step shows that this final step is very effective at removing large carbon particles and even larger carbon nanotubes bundles. For example, Y_D for the HNO_3/DMF increased from ~70% before centrifugation to ~90% after centrifugation. However, for both the HCl/NMP and the HCl/DMF processes, Y_D was not affected by centrifugation ($\Delta Y_D < 5\%$) and remained near 50%; presumably, there were only a few large bundles after sonication in these cases. NearIR−vis−UV OD data were taken before and after the debundling step (in amides). After debundling, we observed a noticeable narrowing and slight downshifting of the van Hove peaks in the OD (see Supporting Information S2 and S3).

Additional attempts were made to change the chemical processing to increase Y_D for the HCl-treated samples, where the attendant wall damage is observed to be less via Raman scattering. To do this, 6 N HCl/H_2SO_4 (3:1) solution was used in the acid-reflux step, and the same process of dispersion, centrifugation, and imaging was completed. Via Raman scattering, the wall damage was not observed to increase by adding the more oxidizing sulfuric acid. The peak position, width, and relative intensity of the R-, D-, and G-bands in the Raman spectra (not shown) were found to be the same for both 6 N HCl- and 6 N HCl/H_2SO_4 (3:1)-refluxed samples. Unfortunately, no change in the dispersion yield, Y_D (~50%), was noticed when H_2SO_4 was added.

The optimal physical properties of organic solvents that dissolve SWNTs are still not well established.[16] Electron pair donicity (Lewis basicity) without hydrogen bond donation, a property present in amide solvents such as DMF and NMP, was found to be a necessary, but not a sufficient, condition for solvating HNO_3-treated SWNTs, because other solvents with the same property have failed to disperse them.[16] DMF and NMP are subject to cleavage of the CH_3−N and C−H bonds under ultrasound excitation,[37] evidencing the nucleophilic character of the N−C−O group and, therefore, increasing the possibility of physi- or chemisorption. The charge-stabilized colloidal nature of the HNO_3-treated SWNT suspension in DMF was also proposed by several authors.[38,39] SWNTs in DMF were found to carry ~1 negative charge every 3.5 nm of length by measurements of ζ potential in electrophoretic mobility experiments.[40] The interactions between these anionically charged SWNTs in electrolyte solution before the critical coagulation concentration were found to be described by a simple model of solid spheres with van der Waals and electric double-layer interactions.[38]

The difference between the high percentage of individual tubes dispersed in amide solvents from using HNO_3-treated samples and that using HCl-treated samples (Figure 5a−c) might be explained by the effective interaction between the solvent and the respective (functionalized) tube surface. It is known that nitrogen-containing functional groups, such as amines and amides, possess significant affinity for physi- or chemisorption with attendant weak charge transfer on the SWNT sidewalls due to the high nucleophilicity of these N-based groups, as mentioned above. In HCl-refluxed samples, Raman spectra indicate that the wall damage is almost not detectable. This indicates that functionalization of the SWNT wall with oxygen-containing functional groups is not expected to be extensive. Hence, the amide adsorption on the nanotube wall, stabilized by the donation of π-electrons from the aromatic rings to the N-based electronegative solvents, should be the dominant interaction that drives the tube debundling. After refluxing in 3 N HNO_3, the pristine tube walls are functionalized with hydroxyl and carboxyl groups.[41] A dipolar interaction between the solvent and these polar groups may also provide a significant benefit to dissolution, consistent with the higher values of $Y_D \approx 90\%$ we observe for HNO_3-processed tubes. We also suggest that polar groups added on the nanotube walls, for example, −COOH groups, may provide a second mechanism for the debundling process.

In one experiment, to investigate the effects of HNO_3-reflux on debundling, we annealed a dry oxidized/HNO_3-refluxed SWNT sample at 1100 °C in 10^{-6} Torr for 1 h (the Raman spectrum for this annealed sample is also shown in Figure 2e, and the spectrum exhibited very narrow SWNT bands and the D-band decreased). We then tried to disperse this annealed and still bundled SWNT material in amides (DMF and NMP) using ultrasound (by our usual procedure). We found that the purified and high-T annealed material dispersed much less efficiently. We expect that this 1100 °C vacuum annealing should reduce significantly the tube wall functionalization,[41] and the narrowing of the Raman lines is in agreement with this expectation. Therefore, it appears that tube wall functionalization, prior to the debundling step, is important. As we have mentioned above, the functionalization may separate the tubes in the bundle, reducing the van der Waals interaction; it may also be that the functional groups enhance the SWNT interaction with the amide solvent.

In Figure 5d−f, we exhibit the length distributions for the debundled tubes obtained from AFM z-scan analysis. The samples investigated are the same as in Figure 5a−c. First, we can see that for the case of HCl-reflux, there is no significant difference in the final length distribution depending on whether NMP or DMF was used with ultrasound to disperse the tubes. Second, HNO_3-reflux was found to reduce the average tube length from ~800 nm for HCl-reflux to ~300 nm, similar to lengths found previously for laser oven tubes sonicated in DMF.[36] On the basis of our AFM studies, we suggest that the final tube length from sonication in solvent depends significantly on the acid processing. This processing functionalizes the tube wall or creates defects (missing C-atoms) in the tube wall (as seen by Raman scattering), and these positions in the tube wall appear to locate "weak" positions at which the ultrasonic cutting can occur.

Monthioux et al. using HRTEM studied the effects of HNO_3 refluxing and sonication on the structural integrity of the tubes. Their laser oven tube soot was refluxed in 3 N HNO_3 solution for 45 h (~3× longer than in this study) and then sonicated in DMF.[18] Much different from the results presented here, they did not report exceptional dissolution or debundling of their laser oven tube bundles in DMF. Consistent with our Raman results (Figure 3), they reported that the HNO_3-refluxed material

(37) Liche, J.-L. *Synthetic Organic Sonochemistry*; Plenum Press: New York, 1998.
(38) Sano, M.; Okamura, J.; Shinkai, S. *Langmuir* **2001**, *17*, 7172.
(39) Sano, M.; Kamino, A.; Okamura, J.; Shinkai, S. *J. Inclusion Phenom. Macrocyclic Chem.* **2001**, *41*, 49.
(40) Boul, P. J.; Liu, J.; Mickelson, E. T.; Huffman, C. B.; Ericson, L. M.; Chiang, I. W.; Smith, K. A.; Colbert, D. T.; Hauge, R. H.; Margrave, J. L.; Smalley, R. E. *Chem. Phys. Lett.* **1999**, *310*, 367.
(41) Kim, U. J.; Liu, X.; Furtado, C. A.; Gutierrez, H. R.; Eklund, P. C., to be submitted.

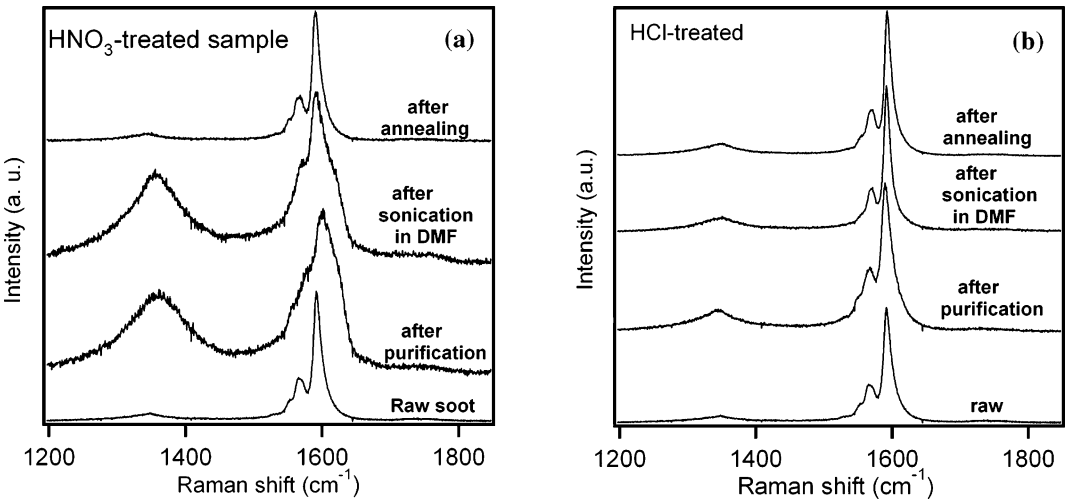

Figure 6. Effects of purification and dispersion on the Raman spectrum of arc-derived SWNTs. The spectra shown are (bottom) raw soot, (middle) soot after dry oxidation and acid reflux, after sonication, (top) after high-temperature (1100 °C) annealing under vacuum (10^{-6} Torr). (a) and (b) refer, respectively, to HNO_3- and HCl-reflux. There is an arbitrary vertical.

appears very heterogeneous. More important for this study, they reported a dramatic structural degradation in the tube wall structure. In their HRTEM images, they interpret the disappearance of evenly spaced fringes representing the tube walls within the rope as clear evidence for strongly damaged, distorted, and segmented tubes. They also found that the structure was improved after the ropes were vacuum annealed at 1200 °C for 14 h. After sonication of their 3 N HNO_3-refluxed SWNT sample in DMF for at least 15 h, Montrioux et al. found that the ultrasonic treatment induced extensive further damage, with many of the ropes transformed into an amorphous material.[18] Many SWNTs survived the ultrasonic dispersion, but they appeared segmented or exhibited many holes in the walls. This level of damage appears to be much more severe than what we observed via Raman scattering in this study (for ultrasonic dispersion in DMF) (Figure 6). That is, the molecular character of the tube remains in our vibrational spectra, as discussed further below. However, they refluxed for a factor of 3× longer.

In Figure 6, we compare the Raman spectra of the nanotubes before and after sonication in DMF; the spectrum of the raw soot is shown for comparison. In Figure 6a, we show results for dry oxidation/HNO_3-reflux purification, and in Figure 6b are the results for dry oxidation/HCl-reflux purification. Centrifugation was performed on the sonicated liquid before the Raman spectrum was collected on tubes removed from the supernatant liquid. As already discussed (cf., Figure 2), the much stronger attack of HNO_3 on the tube walls is clearly evident in Figure 6. However, the effects of sonication are, comparatively speaking, very subtle. In both the HCl and the HNO_3 cases, a slight narrowing of the G-band components and D-band is observed, probably indicating that the centrifugation removed small amounts of other disordered sp^2 carbons still present after purification. Most important is the clear observation that sonication certainly does not broaden the Raman features; that is, we see no Raman evidence for wall damage during the sonication/dispersion step. Thus, it is clear from Raman spectroscopy that HNO_3 damage is much more severe than that caused by ultrasonic processing in DMF. The same results were found for ultrasonic processing in NMP; that is, no noticeable damage via the G- and D-band was observed. As shown in Figure 6a, annealing at 1100 °C under vacuum (10^{-6} Torr) restores order in the tube wall of a dry oxidized/HNO_3-treated/DMF sample. However, in the case of HCl treatment, no Raman evidence for wall functionalization or wall damage was observed before, or after, amide processing in ultrasound. Therefore, after an 1100 °C vacuum annealing, the samples given the dry oxide/HCl/DMF treatment exhibited little or no change in the Raman line shape (Figure 6b).

Some comments about the Raman-active radial breathing modes and chemical processing are worth making here. For HCl-treated samples, we saw a downshift of 3 cm^{-1} for the SWNT radial (R) band after purification (from 161 (raw) to 158 cm^{-1} (purified)) and then an upshift of 6 cm^{-1} in relation to the purified sample (from 158 (purified) to 164 cm^{-1} after the tubes were dispersed as isolated tubes in solution). Several theoretical calculations have indicated that the tube−tube interaction in the bundle upshifts the R-band frequency by ∼12−14 cm^{-1} for tubes with diameters in the range 1.2−1.6 nm. So the upshifting we observe by debundling is an opposite effect to what has been predicted theoretically. This upshifting upon debundling has been reported earlier and attributed to a change in the resonance scattering.[42]

It is interesting to compare Raman scattering and electron microscopy as probes of wall damage during purification and during debundling. In Figure 7, we display HRTEM images of bundles of SWNTs that have been subjected to dry oxidation and acid reflux: 16 h 3 N HNO_3-reflux (Figure 7a) and 24 h 6 N HCl-reflux (Figure 7b). The samples were neutralized in NaOH as discussed above. Whereas the Raman spectra of these purified materials show a clear difference due to wall damage (cf., Figures 2, 3, and 6), the HRTEM evidence for damage is more subtle, but nevertheless evident. A close inspection of both images in Figure 7 reveals that the fringes associated with the triangular rope lattice are much more distinct and straight after HCl-reflux (Figure 7b) than after HNO_3-reflux (Figure 7a). Furthermore, notches can be seen to form in the wall of tubes that are on the outside of the bundle (see arrows in Figure 7a).

In Figure 8, we display isolated tubes produced from ultrasonic dispersion in DMF: Figure 8a,b, HNO_3 purification;

(42) Rao, A. M.; Chen, J.; Richter, E.; Schlecht, U.; Eklund, P. C.; Haddon, R. D.; Venkateswaran, U. D.; Kwon, Y.-K.; Tománek, D. *Phys. Rev. Lett.* **2001**, *86*, N17, 3895.

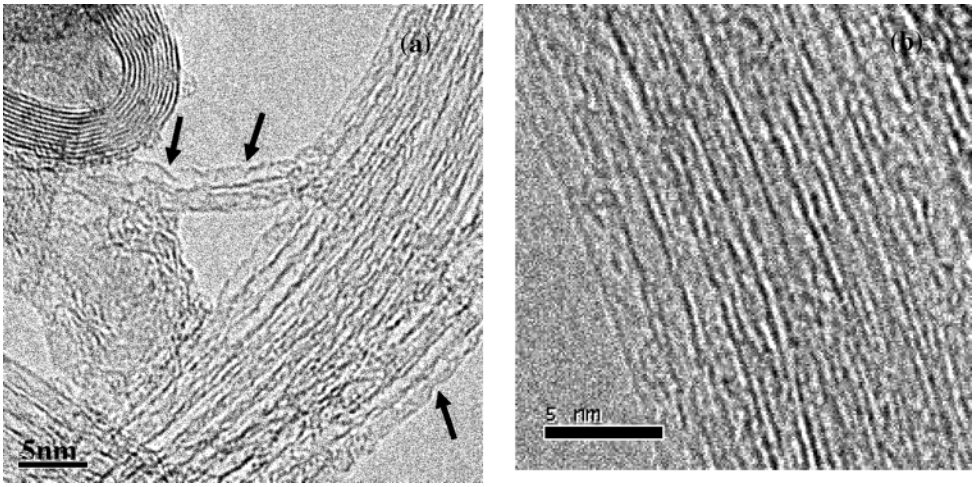

Figure 7. (a) HRTEM image of HNO_3-refluxed bundles dispersed in 2-propanol, (b) HCl-refluxed bundles after dry oxidation in 2-propanol.

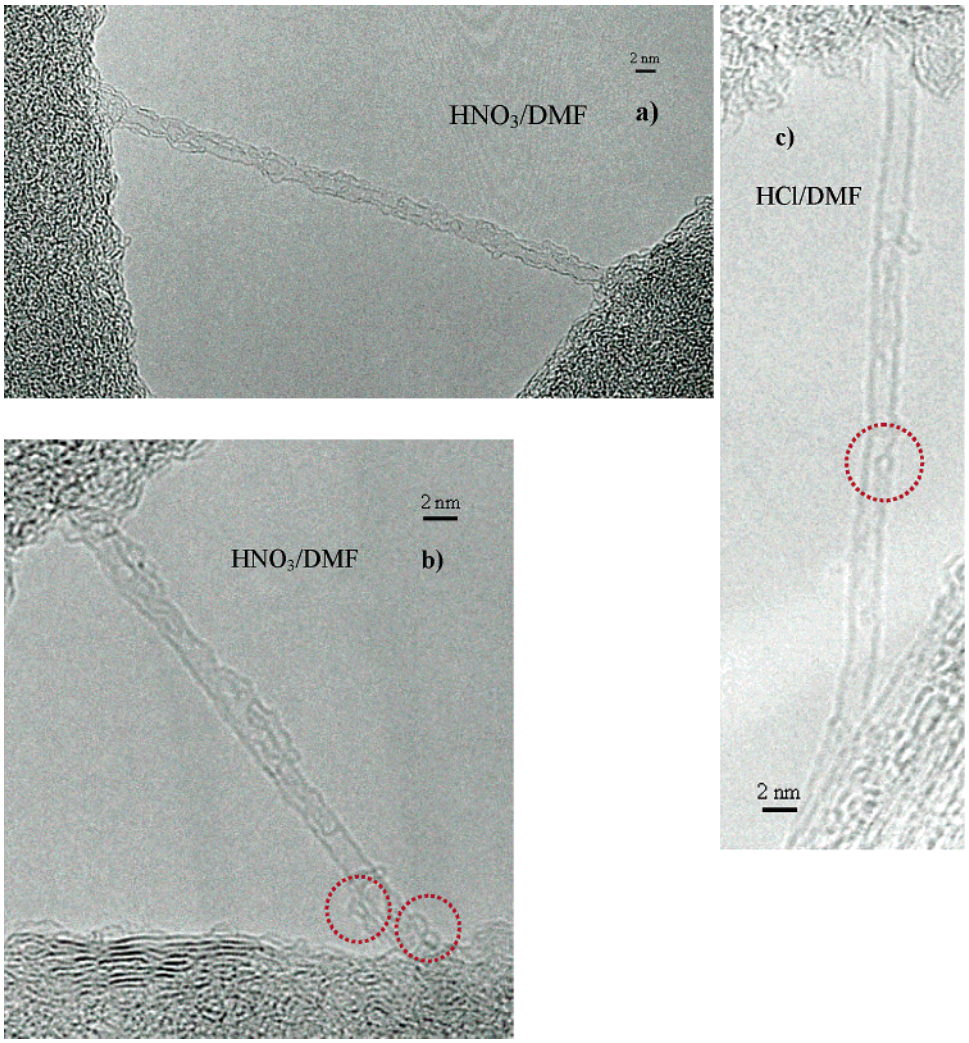

Figure 8. (a,b) HRTEM images of debundled SWNTs dispersed in DMF after HNO_3-reflux, (c) SWNTs dispersed in DMF after HCl-reflux. All samples were subjected to the sample dry oxidation and centrifugation steps. The HNO_3-refluxed tubes (a,b) appear to be coated with carbon sheet fragments; closed-shell structures are inside the circles.

Figure 8c, HCl purification. In all cases, we performed the initial dry oxidation and the final centrifugation in the same way, as described above. The acceleration voltage in the microscope was 100 kV, that is, the same as that used by Monthioux et al.[18] First, we can see that the wall of the HCl-purified tube is cleaner, that is, has less carbon fragments, fullerenes, etc. attached to it, than the tube walls subjected to HNO_3-reflux. This coating by carbon fragments probably does not affect the nanotube Raman spectrum, although the fragments may contribute to D-band scattering and a broad G-band contribution superimposing with the nanotube G-band. Second, the HRTEM images show that the tube wall of the HCl-refluxed tube appears

straighter; yet it is not perfectly straight. Monthioux et al. have proposed that defects on the tube wall make the tube more susceptible to electron beam damage.[18] They reported that a defective tube wall structure or occurrence of some reactive reaction product on the tube surface accentuates the sensitivity of the wall to the electron beam and allows the tube wall to rapidly kink, distort, and/or segment within a time period of 5−20 s. We were unable to directly support this by our HRTEM study, as we did not find images of isolated tubes before chemical processing for comparison. However, our Raman scattering data on isolated, HCl-purified tubes seem to be consistent with their proposal, in that if the tubes were as imperfect as that observed in the HRTEM image of Figure 8c, then we would expect broadened Raman bands for this material.

We mention again that the HCl-purified isolated nanotube material exhibits a Raman spectrum whose line widths are as narrow as those found in the raw soot. Thus, it is interesting to consider the possibility as proposed by Monthioux et al. that even at 100 keV acceleration potential, functionalized nanotubes, or nanotubes with small defects, are subject to large wall rearrangement reactions driven by the electron microscope beam. Closed-shell structures appear to be present on the tube walls in Figure 8b and c (inside the circles). Monthioux et al.[18] also observed C_{60} molecules on the nanotube wall (their tubes were grown by the pulsed laser vaporization technique). The closed-shell structures that appear to be on the surface of our tubes may be created during arc-discharge growth, or are some reaction product from purification, ultrasonic dispersion, or they might be generated in the electron beam. We see no evidence in the Raman spectra of their existence, which means they are probably not present at the ∼1%, or greater, level.

Finally, we attempted to directly observe (via HRTEM) a reversal in the wall damage created via acid reflux (recall that Raman scattering shows no evidence for wall damage via ultrasonic dispersion in the amides). First, we deposited a few drops of debundled SWNT in DMF on a Si substrate. These tubes had been subjected to an aggressive HNO_3-reflux, and the Raman bands were significantly broadened. The tubes on the Si/SiO_2 substrate were annealed at high temperature (1100 °C, 10^{-6} Torr, 1 h). After this annealing step, we sonicated the SWNTs in ethanol to remove the SWNTs from the substrate for HRTEM study. We did observe the structural restoration of the tube wall, consistent with the Raman experiments (see Supporting Information S4). However, our overall impression is that Raman scattering affords a much more sensitive probe of wall damage. In the HRTEM images, the quality of the tube wall on the atomic scale is almost impossible to observe. Only the restoration of significant tube wall defects (e.g., ∼0.5 nm diam holes) can be readily observed in HRTEM.

Summary and Conclusions

Our results show that the details of the oxidation and metal digestion step (e.g., HCl or HNO_3) by which the metal catalyst and amorphous carbon are removed are a crucial first step to debundling and high dispersion yield, but this step can also significantly impact the structural quality of the debundled isolated tubes. This is perhaps a little surprising, as many of the tubes in the interior of the bundle might be viewed as protected from the acids or oxidative cleanup by the outer tubes in the bundle. Nevertheless, this is what we have observed.

Although the use of ultrasonic dispersion in amide solvents such as DMF and NMP might be expected to lead to considerable damage to the tube wall structure, we do not see evidence for this damage in this work.

We have shown that a processing scheme involving a 3 N HNO_3-reflux can yield a final product with as much as 90% isolated tubes in amide solution. Tubes can be deposited from this solution onto substrates where they can be subsequently vacuum annealed at 1100 °C to repair much of the wall damage induced in the chemical processing. We believe that this is an important result, because their deposition can be controlled in such way that isolated nanotubes can, for example, be positioned at specific locations and with a specific orientation on the substrate.[17]

Acknowledgment. This work was supported by NSF-DMR-0103585 and NSF-DMR-0304178, and the PSU MRSEC-DMR-0213623. C.A.F. acknowledges financial support from CNPq-Brazil. We also would like to thank Dr. B. K. Pradhan for many stimulating discussions, and Gugang Chen for assistance with the Raman scattering experiments.

Supporting Information Available: S-1: Comparison of the optical density of raw SWNT soot (arc process). S-2: Optical density of SWNTs before (dotted line) and after (solid line) debundling in NMP. S-3: Optical density of SWNTs before (dotted line) and after (solid line) debundling in DMF. S-4: HRTEM image of an individual SWNT subjected to dry oxidation, then aggressive HNO_3-reflux and ultrasonic debundling in DMF followed by annealing at 1100 °C in a vacuum. This material is available free of charge via the Internet at http://pubs.acs.org.

JA039588A